Supporting information

Tuning MIP-QCM Selectivity for Zinc Ions via Cross-linker/Monomer Ratio

Jialing Song [a], Charles Jordi Windle [b], Haoxing Lai [c], Melvin Zhi Yuan Low [d], Fun Man Fung [e*], Xuan Hao Lin [f*], Sam Fong Yau Li [f,g*]

[a] International Joint Laboratory Catalyst Chemistry, Department of Chemistry, College of Science, Shanghai University, Shanghai 200444, China
[b] Yusuf Hamied Department of Chemistry, University of Cambridge, Lensfield Rd, Cambridge CB2 1EW, United Kingdom
[c] Yong Loo Lin School of Medicine, National University of Singapore, Singapore 117597, Singapore
[d] School of Computing, NUS School of Computing, COM1, 13, Computing Dr, Singapore 117417, Singapore
[e] School of Chemistry, University College Dublin, Belfield, Dublin 4, D04 C1P1 Ireland
[f] Department of Chemistry, National University of Singapore, 3 Science Drive 3, Singapore 117543
[g] NUS Environmental Research Institute (NERI), #02-01, T-Lab Building (TL), 5A Engineering Drive 1, Singa-pore 117411, Singapore
*Correspondence: Tel.: +65 6515 2681; fax: +65 6779 1691. Email address: chmlifys@nus.edu.sg (Sam F. Y. Li).

Contents

1. Materials and Reagents

All chemicals were of analytical reagent grade and used without any further purification.

2. Experimental Section

2.1. Composition and Principle of MIP

MIP is a complex and sophisticated molecular structure system, primarily composed of four key components: functional monomers, comonomers, cross-linkers, and template molecules. Among these, functional monomers serve as the core components enabling MIP to exert its molecular recognition function. Their structures are highly complementary to the template molecule (zinc ions in this study) in terms of shape and size.

During the synthesis of MIP, the process begins with the formation of a stable template-monomer complex. This complex is formed through intermolecular forces such as hydrogen bonds, electrostatic attractions, and van der Waals forces between the template molecule and multiple complementary functional monomers. The formation of this complex is analogous to leaving a unique imprint on a malleable material, laying the foundation for the subsequent construction of specific recognition sites. Subsequently, the cross-linker plays a crucial role. It promotes the polymerization reaction among functional monomers, connecting individual functional monomers to form a three-dimensional polymer network structure.[1] This cross-linking not only polymerizes the functional monomers but, more importantly, endows the entire polymer network with sufficient stability. This stability ensures that after the template molecule is eluted, the cavity structure within the polymer network remains intact without collapse or deformation.[2]

Once the template molecule is successfully eluted from the organic polymer matrix, a series of specific recognition sites and cavities that are highly matched to the template molecule in terms of charge distribution, geometric shape, and size are left within the polymer network.[3] The formation of these specific recognition sites and cavities is attributed to the unique position distribution of functional groups

complementary to the template within the polymer network and the corresponding defined intermolecular attractions.[4, 5] These features enable MIP to precisely recognize and capture the template molecule.

2.2. Experimental Section

In this study, the selection of functional monomers was meticulously considered and screened. MAA (methacrylic acid), due to its distinctive chemical structure and properties, was chosen as one of the functional monomers. MAA contains a carboxyl group, which can act as both a hydrogen-bond donor and a proton donor. Additionally, it has a double-bond structure that allows it to participate in polymerization reactions. Moreover, its carboxyl group can function as a hydrogen-bond acceptor, enabling it to form various types of intermolecular interactions with the template molecule or other functional monomers.[4, 6]14 These interactions provide a crucial chemical foundation for the specific recognition of MIP. Besides MAA, DMPAPS (N,N-dimethyl-N-(methacrylamidopropy)-n-(3-sulfopropyl)-ammonium betaine) and HEMA (2-hydroxyethyl methacrylate) were also incorporated into the category of functional monomers. DMPAPS and HEMA possess special functional groups that can effectively chelate or coordinate zinc ions through ionic interactions, thereby further enhancing the specific binding ability of MIP to zinc ions.

EGDMA (ethylene glycol dimethacrylate), serving as a cross-linker, plays a vital role in the synthesis of MIP. EGDMA has a similar structure to MAA and HEMA, which enables it to better integrate and synergize with functional monomers during the polymerization reaction. Through cross-linking with functional monomers, EGDMA endows MIP with structural rigidity, orderliness, and more efficient binding sites.[7] This ensures that MIP can maintain a stable structure and high-efficiency recognition performance in complex detection environments. AIBN (azobisisobutyronitrile) is employed as an initiator for the free-radical polymerization reaction.[8] Under certain conditions, it decomposes to generate free radicals, which initiate the polymerization reaction between functional monomers and cross-linkers, facilitating the formation of MIP.

Acetonitrile is added to the reaction system as a porogen. Its function is to artificially create pore structures within the polymer network.[9] These pore structures are of great significance for enhancing the selectivity and rebinding ability of the MIP sensor.[10] They provide channels for the diffusion and binding of template molecules, increasing the contact area between MIP and template molecules, and thus improving the detection sensitivity and accuracy.

Furthermore, zinc acetate dihydrate was utilized as the template molecule, 1-hexanol was used to disperse the polymer, methanol served as the reaction solvent, nitric acid was employed to desorb zinc ions, and zinc solutions were used to evaluate the performance of MIP.

2.3. Optimized Polymer Synthesis Design Procedure

When conducting polymer synthesis, the optimized experimental procedures were strictly adhered to ensure the accuracy and reproducibility of the experimental results. Firstly, a 1.5-mL Eppendorf tube was prepared. In the tube, 11.7 mg (40 μmol) of DMPAPS and 2.2 mg (10 μmol) of zinc acetate dihydrate were accurately added and then dissolved in 0.5 mL of methanol. Methanol, as an excellent solvent, can fully dissolve DMPAPS and zinc acetate dihydrate and uniformly disperse them in the solution, creating favorable conditions for the smooth progress of subsequent reactions.

Subsequently, 3.37 μL of MAA, 4.87 μL of HEMA, 32.39 μL of EGDMA, and 1.09 μL of AIBN were added to the solution in sequence. During the addition of these reagents, precise measurement was essential to guarantee the accurate proportion of each component in the reaction system. After adding the reagents, the reaction system was placed in an inert nitrogen atmosphere and mixed for 5 minutes. The purpose of this step was to expel the oxygen inside the tube. Since oxygen is an inhibitor of the free-radical polymerization reaction and can hinder the progress of the polymerization reaction, nitrogen was introduced to displace the oxygen, providing an oxygen-free reaction environment for the polymerization reaction.[11]

Under anaerobic conditions, 0.3 mL of ACN (acetonitrile) was added. As a porogen, ACN can form pore structures in the polymer network during the subsequent

polymerization process. After adding ACN, the resulting solution was stirred to ensure thorough mixing and then heated and maintained in a 70 °C constant-temperature water bath for 3 h. During these 3 h of reaction, AIBN decomposed to generate free radicals, initiating the polymerization reaction between functional monomers and cross-linkers and gradually forming MIP with a specific structure.

After the reaction was completed, the solution was centrifuged at 5000 revolutions per minute for 3 minutes. The purpose of centrifugation was to precipitate the polymer and separate it from other impurities in the reaction solution. After centrifugation, the precipitate was washed twice with 0.5 mL of ACN to further remove residual impurities and unreacted reagents on the surface of the precipitate. After the washing process, the precipitate was dispersed in 1 ml of 1-hexanol. 1-hexanol can effectively disperse the polymer, enabling it to form a homogeneous suspension. Finally, 9.6 μL was extracted from the 1-hexanol mixture for subsequent use.

For the purpose of conducting comparative experiments, non-imprinted polymers (NIPs) were synthesized using the same method. The only difference was that zinc acetate dihydrate template was not added during the synthesis process. By comparing the differences in detection performance between MIP and NIPs, the specific recognition ability of MIP for zinc ions could be more accurately evaluated.

2.4. Data Measurement and Characterization

In this study, a quartz crystal microbalance (QCM) was employed as the primary tool for data measurement and characterization. QCM is a high-resolution mass-sensing instrument. Diagrams of the QCM and the quartz crystal are found in Figure S3 and Figure S4. When used in combination with MIP, an extremely sensitive MIP-QCM sensor can be constructed, which is capable of precisely measuring zinc-ion concentrations at the parts-per-billion (ppb) level.[12] The working principle of QCM is based on the inverse piezoelectric effect. When a mechanical stress is applied to a quartz crystal, it causes a relative displacement between the positive and negative charge centers inside the quartz crystal, generating an external electric field on the crystal surface. When an alternating-current voltage that interacts with the external

electric field is applied to the crystal surface, the crystal chip oscillates at its inherent resonant frequency. In the MIP-QCM sensor, the adsorption and desorption processes of MIP for Zn^{2+} cause minute changes in the mass of the sensor chip. There is a well-defined relationship between this mass change and the frequency change of the sensor chip, which is described by the Sauerbrey equation[13]:

$$\Delta f = -\frac{2f_0^2 \Delta m}{A\sqrt{\rho_q \mu_q}}$$

Where, Δf represents frequency change (Hz), Δm represents change in mass (g), f_0 represents resonant frequency of fundamental mode of crystal (5 MHz), A represents piezoelectrically active area (cm^2), ρ_q represents density of quartz (2.648g cm^{-3}), and μ_q represents shear modulus of quartz (2.947×10^{11} g cm^{-1} s^2).

However, the Sauerbrey equation holds under certain assumptions. One of the assumptions is that the added polymer-solution layer can be approximated as part of the oscillating crystal chip itself. To ensure the validity of this assumption, in experimental operations, a layer of MIP suspension less than 10.0 μL is uniformly coated on the chip, and the chip is dried overnight before use. The purpose of this is to enable the MIP suspension to adhere firmly to the crystal surface, forming a uniform and stable polymer film, thus meeting the application conditions of the Sauerbrey equation.

When monitoring the affinity of the MIP-QCM sensor for zinc ions, first, the crystal chip is mounted on the QCM electrode. Then, deionized water is slowly introduced into the flow cell through a peristaltic pump. The introduction of deionized water is to clean the flow cell and the sensor chip, eliminating the interference of external impurities on the detection results and allowing the sensor chip to reach a stable initial state. After the detected resonant frequency becomes stable, a zinc-ion solution is slowly introduced through the peristaltic pump. During the process of zinc-ion adsorption onto the sensor chip, MIP specifically binds to zinc ions, causing an increase in the mass of the sensor chip. According to the Sauerbrey equation, the resonant frequency will decrease accordingly. At this time, by monitoring the change

in the resonant frequency in real-time using a computer, the adsorption information of zinc ions can be accurately obtained. Subsequently, a 0.01N nitric-acid solution is introduced. The acidic property of nitric acid is used to desorb the zinc ions adsorbed on MIP, and the desorption process lasts for 2 minutes. After the desorption is completed, the sensor chip is washed with deionized water for 20 minutes to thoroughly remove the residual nitric acid and zinc ions on the chip surface.

To ensure the accuracy and reliability of the experimental results, at least three repeated cycle tests are required for different test variables. The key test variables include zinc-ion solutions with different concentrations (50, 200, 500, 1000, 2000 ppb) and solutions of other metal cations (Cu^{2+}, Ni^{2+}, Co^{2+}, Mg^{2+}). During the testing process, the flow-rate control parameter is set to a constant value of 150 μL/min to ensure a stable flow state of the solution in the flow cell and avoid the influence of flow-rate changes on the detection results.

In addition, to verify the specific recognition ability of the MIP-QCM sensor for zinc ions, a sensor chip coated with NIPs is used as a negative control, and the same tests are performed on various solutions. By comparing the detection results of the MIP-QCM sensor and the NIPs-QCM sensor under different test variables, the specific recognition performance and anti-interference ability of MIP for zinc ions can be clearly evaluated.

3. Figures and Table

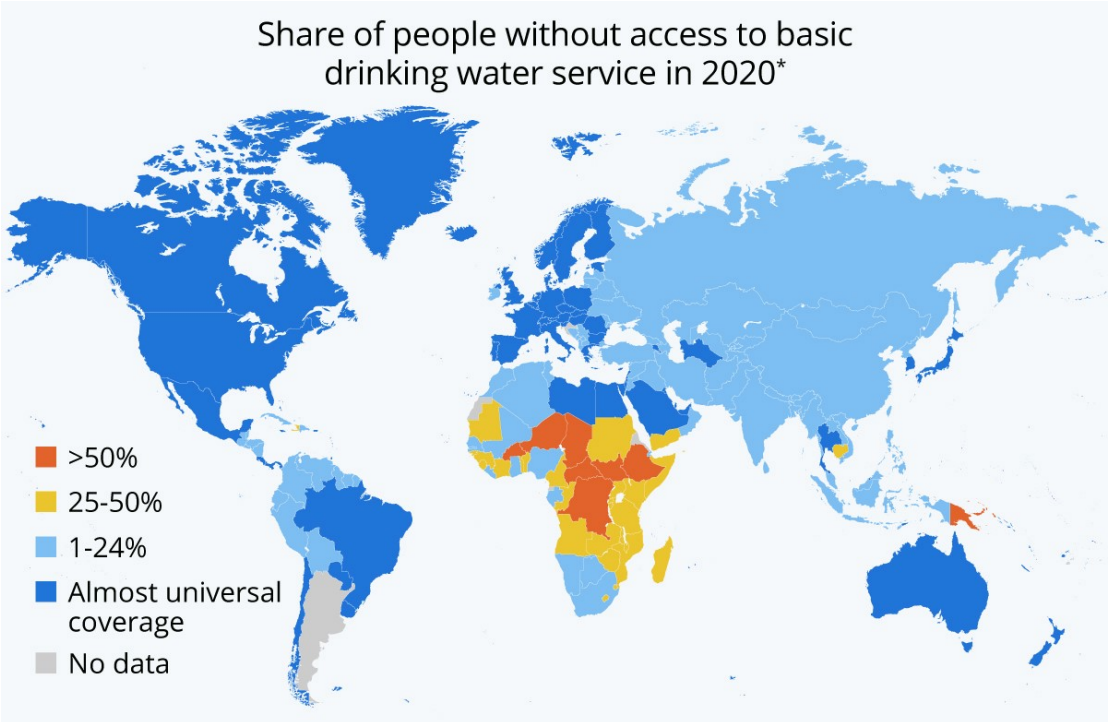

Figure S1. The percentage of population drinking from contaminated water sources worldwide. In 41 countries, more than 1 in 5 people obtain their drinking water from a water source polluted by heavy metals. Reproduced with permission from statista[14].

Product type	Ag	As	Cd	Co	Cr	Cu	Hg	Ni	Pb	Se	Zn
Amalgam fillings and thermometers							✓				
Cleaning products					✓	✓					
Cosmetics, shampoos			✓				✓	✓	✓	✓	✓
Disinfectants							✓				
Fire extinguishers											
Fuels						✓	✓		✓		✓
Inks						✓				✓	
Lubricants					✓				✓		✓
Medicines and Ointments		✓		✓		✓	✓				✓
Health supplements				✓	✓	✓				✓	✓
Food products		✓		✓		✓			✓		✓
Oils and lubricants					✓	✓			✓		✓
Paints and pigments		✓	✓	✓	✓	✓	✓	✓	✓	✓	✓
Photographic	✓				✓		✓				
Polish	✓					✓					✓
Pesticides and gardening products			✓		✓	✓	✓		✓		
Washing powders			✓						✓		✓
Wood-preservatives		✓				✓			✓		
Water treatment and heating systems			✓			✓		✓	✓		✓

Source: https://ec.europa.eu/environment/archives/waste/sludge/pdf/sludge_pollutants_2.pdf

Figure S2. Wide industrial and commercial uses of zinc in comparison to other heavy metals. (Source: https://ec.europa.eu.)

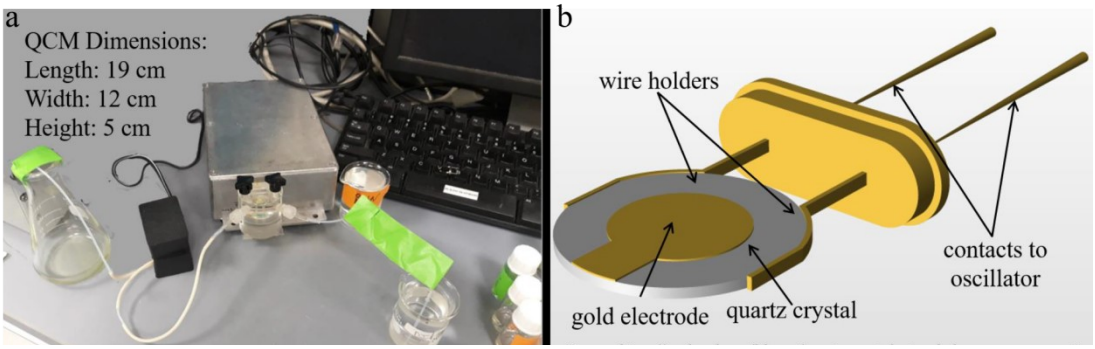

Figure S3. QCM setup. (a) QCM analyser connected to a computer. (b) Quartz crystal chip connected to the QCM analyser.

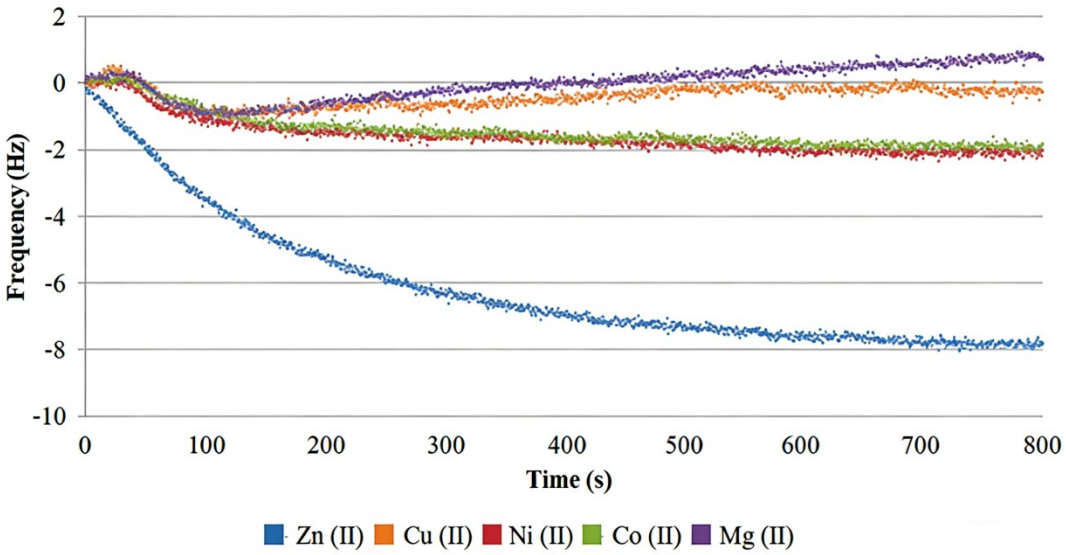

Figure S4. Selectivity of various ions tested on MIP. QCM analyser connected to a computer.

```
---------------
TOTAL SCF ENERGY
---------------

Total Energy     :      -304.45201284 Eh       -8284.56045 eV

Components:
Nuclear Repulsion :       226.98880495 Eh        6176.67940 eV
Electronic Energy :      -531.44081779 Eh      -14461.23985 eV
One Electron Energy:     -865.13299516 Eh      -23541.46562 eV
Two Electron Energy:      333.69217737 Eh        9080.22578 eV

Virial components:
Potential Energy  :      -607.43937376 Eh      -16529.26569 eV
Kinetic Energy    :       302.98736092 Eh        8244.70524 eV
Virial Ratio      :         2.00483404
```

```
--------------
SCF CONVERGENCE
--------------

  Last Energy change         ...  -1.2017e-09  Tolerance :  1.0000e-08
  Last MAX-Density change    ...   3.1230e-06  Tolerance :  1.0000e-
07
  Last RMS-Density change    ...   1.3978e-07  Tolerance :  5.0000e-09
  Last Orbital Gradient      ...   1.7201e-06  Tolerance :  1.0000e-05
  Last Orbital Rotation      ...   3.8915e-06  Tolerance :  1.0000e-05

          **** THE GBW FILE WAS UPDATED (MAA4.gbw) ****
          **** DENSITY FILE WAS UPDATED (MAA4.scfp.tmp)
****
          **** ENERGY FILE WAS UPDATED (MAA4.en.tmp) ****
```

Figure S5. ORCA Script about energy values for MAA.

Timings for individual modules:

Sum of individual times ... 3229.983 sec (= 53.833 min)
GTO integral calculation ... 30.502 sec (= 0.508 min) 0.9 %
SCF iterations ... 30.502 sec (= 0.508 min) 0.9 %
SCF iterations ... 1989.071 sec (= 33.151 min) 61.6 %
SCF Gradient evaluation ... 1187.055 sec (= 19.784 min) 36.8 %
Geometry relaxation ... 23.355 sec (= 0.389 min) 0.7 %

******ORCA TERMINATED NORMALLY******

TOTAL RUN TIME: 0 days 0 hours 54 minutes 12 seconds 199 msec

Figure S6. ORCA Script about timings for simulations.

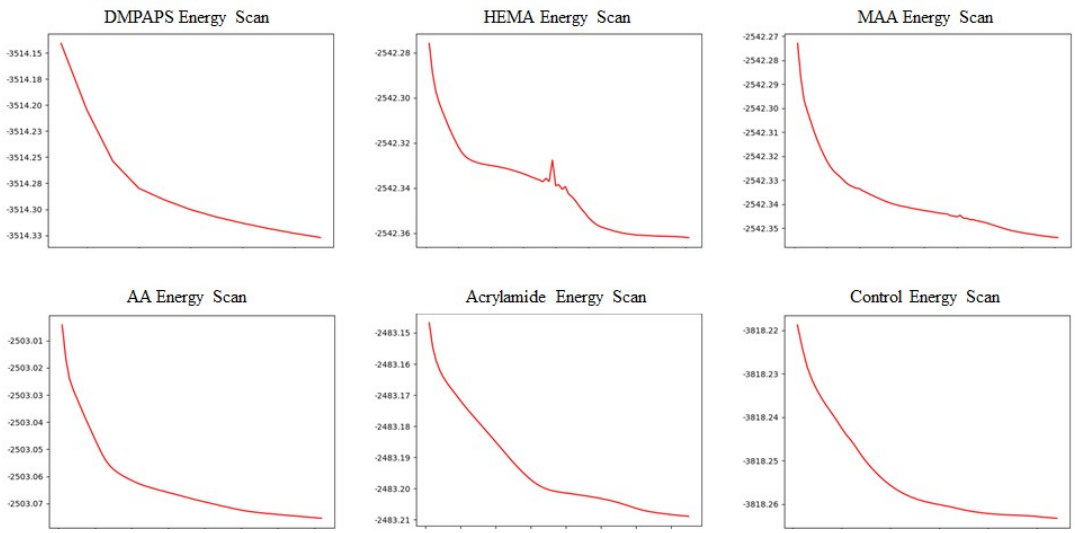

Figure S7. Matplotlib Energy Scans. Values taken at last iteration where energy value has converged.

Table S1. A comparison of various analytical methods for trace metals in water.

	AAS	AFS	Electrochemical	MIP
Portability	NO Complex	NO	Yes Complex[16]	Yes
Operation/Set-up	Samples have to be pretreated to destroy organic matter and other contaminants[15]	Easy	Separation and analytical procedures require qualified operators[17, 18]	Easy
Reproducibility of results	High	Moderate Subject to scattering of light[19]	Poor Variance due to frequent electrode polishing[20, 21]	High
Limit of detection	$\times 10^{-6}$ g/L	$\times 10^{-5}$ g/L	$\times 10^{-4}$ g/L	$\times 10^{-5}$ g/L

Table S2. Binding energies of the functional monomers with zinc template, ranked from strongest to weakest.

Functional monomer tested	Binding Energy ΔE_{bind}/Hartree
DMPAPS	3496.866
HEMA	2683.538
MAA	2533.237
AA	2492.735
Acrylamide	2472.874
Control (Argon)	0.002004

Table S3. The performance of different monomer systems

Functional monomer	Selectivity (%)	Sensitivity (ppb/Hz)	LOQ (ppb)	R^2
MAA	62.5	32.8	89.3	0.9762
HEMA	48.7	24.3	112.6	0.9589
DMPAPS	59.2	30.5	95.7	0.9691
MAA/HEMA/DMPAPS （1:1:1 molar ratio）	99.8	51.9	38.1	0.9985

Reference

1. Yanti; Nurhayati, T.; Royani, I.; Widayani; Khairurrijal; Iop In *Synthesis and characterization of MAA-based molecularly-imprinted polymer (MIP) with D-glucose template*, 6th Asian Physics Symposium (APS), Bandung, INDONESIA, Aug 19-20; Bandung, INDONESIA, 2015.

2. Vasapollo, G.; Del Sole, R.; Mergola, L.; Lazzoi, M. R.; Scardino, A.; Scorrano, S.; Mele, G., Molecularly Imprinted Polymers: Present and Future Prospective. *International Journal of Molecular Sciences* **2011,** *12* (9), 5908-5945.

3. Fu, Y.; Finklea, H. O., Quartz crystal microbalance sensor for organic vapor detection based on molecularly imprinted polymers. *Analytical Chemistry* **2003,** *75* (20), 5387-5393.

4. Yan, H. Y.; Row, K. H., Characteristic and synthetic approach of molecularly imprinted polymer. *International Journal of Molecular Sciences* **2006,** *7* (5-6), 155-178.

5. Ji, S. Q.; Esfahani, I. C.; Yang, R. B.; Sun, H. W., Adsorption and Morphology Analysis of Bovine Serum Albumin on a Micropillar-Enhanced Quartz Crystal Microbalance. *Journal of Physical Chemistry B* **2024**, DOI:10.1021/acs.jpcb.4c03393.

6. Mohammad, N.; Atassi, Y.; Tally, M., Synthesis and swelling behavior of metal-chelating superabsorbent hydrogels based on sodium alginate-g-poly(AMPS-co-AA-co-AM) obtained under microwave irradiation. *Polymer Bulletin* **2017,** *74* (11), 4453-4481.

7. Shoravi, S.; Olsson, G. D.; Karlsson, B. C. G.; Nicholls, I. A., On the Influence of Crosslinker on Template Complexation in Molecularly Imprinted Polymers: A Computational Study of Prepolymerization Mixture Events with Correlations to Template-Polymer Recognition Behavior and NMR Spectroscopic Studies. *International Journal of Molecular Sciences* **2014,** *15* (6), 10622-10634.

8. Mijangos, I.; Navarro-Villoslada, F.; Guerreiro, A.; Piletska, E.; Chianella, I.; Karim, K.; Turner, A.; Piletsky, S., Influence of initiator and different polymerisation conditions on performance of molecularly imprinted polymers. *Biosensors & Bioelectronics* **2006,** *22* (3), 381-387.

9. Esfandyari-Manesh, M.; Javanbakht, M.; Atyabi, F.; Badiei, A.; Dinarvand, R., Effect of Porogenic Solvent on the Morphology, Recognition and Release Properties of Carbamazepine-Molecularly Imprinted Polymer Nanospheres. *Journal of Applied Polymer Science* **2011,** *121* (2), 1118-1126.

10. Saloni, J.; Walker, K.; Hill, G., Theoretical Investigation on Monomer and Solvent Selection for Molecular Imprinting of Nitrocompounds. *Journal of Physical Chemistry A* **2013,** *117* (7), 1531-1534.

11. Lata, K.; Sharma, R.; Naik, L.; Rajput, Y. S.; Mann, B., Synthesis and application

of cephalexin imprinted polymer for solid phase extraction in milk. *Food Chemistry* **2015,** *184*, 176-182.
12. Yang, Z. P.; Zhang, C. J., Designing of MIP-based QCM sensor for the determination of Cu(II) ions in solution. *Sensors and Actuators B-Chemical* **2009,** *142* (1), 210-215.
13. Magna, G.; Belugina, R.; Mandoj, F.; Catini, A.; Legin, A. V.; Paolesse, R.; Di Natale, C., Experimental determination of the mass sensitivity of quartz microbalances coated by an optical dye. *Sensors and Actuators B-Chemical* **2020,** *320*, 128373.
14. Buchholz, K. Unsafe Water Kills More People Than Disasters and Conflicts. https://www.statista.com/chart/17445/global-access-to-safe-drinking-water/.
15. Tariq, S. R.; Shah, M. H.; Shaheen, N.; Khalique, A.; Manzoor, S.; Jaffar, M., Multivariate analysis of selected metals in tannery effluents and related soil. *Journal of Hazardous Materials* **2005,** *122* (1-2), 17-22.
16. Rafiq, K.; Sadia, I.; Abid, M. Z.; Waleed, M. Z.; Rauf, A.; Hussain, E., Scientific Insights into the Quantum Dots (QDs)-Based Electrochemical Sensors for State-of-the-Art Applications. *Acs Biomaterials Science & Engineering* **2024,** *10* (12), 7268-7313.
17. Pujol, L.; Evrard, D.; Groenen-Serrano, K.; Freyssinier, M.; Ruffien-Cizsak, A.; Gros, P., Electrochemical sensors and devices for heavy metals assay in water: the French groups' contribution. *Frontiers in Chemistry* **2014,** *2*, 19.
18. Li, Y. Q.; Kuang, K. D.; Chen, Y.; Chen, X.; Cheng, Q. H.; Li, Y.; Liang, L. J.; Jia, N. Q., Exogenous Coreactant-Free Electrocatalytic Reactive Oxygen Species-Driven Dual-Signal Molecularly Imprinted Electrochemiluminescence Sensor for the Detection of Trenbolone. *Analytical Chemistry* **2025,** *97* (5), 3198-3206.
19. Zou, Z. R.; Tian, Y. F.; Zeng, W.; Hou, X. D.; Jiang, X. M., Effect of variable ultraviolet wavelength and intensity on photochemical vapor generation of trace selenium detected by atomic fluorescence spectrometry. *Microchemical Journal* **2018,** *140*, 189-195.
20. Yang, T.; Yu, R. Z.; Yan, Y. H.; Zeng, H.; Luo, S. Z.; Liu, N. Z.; Morrin, A.; Luo, X. L.; Li, W. H., A review of ratiometric electrochemical sensors: From design schemes to future prospects. *Sensors and Actuators B-Chemical* **2018,** *274*, 501-516.
21. Guo, Z. W.; Feng, H. S.; Swager, T. M., Reversible Electrochemical Sensor for NDMA: Leveraging Molecularly Imprinted Polymers for Enhanced Sensitivity and Selectivity. *Acs Sensors* **2025**, 10(2), 881-885.